



3,5-Bis(diphenylphosphinoethyl)pyrazolate ligand (PNNP^{C2}) and its dirhodium complexes: Comparison with related quadridentate dinucleating diphenylphosphinomethyl (PNNP^{Py}) and phthalazine derivatives (PNNP^{Ph})

Akiko Gondoh, Takashi Koike, Munetaka Akita *

Chemical Resources Laboratory, Tokyo Institute of Technology, R1-27, 4259 Nagatsuta, Midori-ku, Yokohama 226-8503, Japan

ARTICLE INFO

Article history:

Available online 27 February 2011

Dedicated to Professor Wolfgang Keim for his invaluable contribution to organometallic chemistry

Keywords:

Rhodium
Quadridentate ligand
Carbonyl complex
Acetylide complex

ABSTRACT

Dirhodium carbonyl complex with the 3,5-bis(diphenylphosphinoethyl)pyrazolato ligand (PNNP^{C2}), $[(\mu-\kappa^2:\kappa^2\text{-PNNP}^{\text{C2}})\text{Rh}_2(\text{CO})_3]\text{BF}_4$, is prepared and its reactivity is studied as compared with the previously reported 3,5-bis(diphenylphosphinomethyl)pyrazolate (PNNP), $[(\mu-\kappa^2:\kappa^2\text{-PNNP})\{\text{Rh}(\text{CO})_2\}_2]\text{BF}_4$, and 1,4-bis(diphenylphosphinomethyl)phthalazine (PNNP^{Ph}) derivatives, $[(\mu-\kappa^2:\kappa^2\text{-PNNP}^{\text{Ph}})\{\text{Rh}(\text{CO})_2\}_2](\text{BF}_4)_2$. The three quadridentate ligands are different in the size of the central ring and the charge; six-membered ring/neutral (PNNP^{C2}) vs. five-membered ring/mono-negative (PNNP) vs. six-membered ring/neutral (PNNP^{Ph}). The number of the carbonyl ligands (n) in the dirhodium carbonyl complexes, $[(\mu\text{-PNNP})\text{Rh}_2(\text{CO})_n](\text{BF}_4)_x$, is dependent on the dinucleating ligand: $n=2$ (PNNP^{Ph}), 3 (PNNP^{C2}) and 4 (PNNP^{Py}). The three dirhodium carbonyl complexes serve as 4e-acceptors, and their reactivities turn out to be very similar as can be seen from formation of the analogous, unique tetranuclear μ_4 -acetylide $\{[(\mu\text{-PNNP})_2\{\text{Rh}(\text{CO})\}_4(\mu_4\text{-C}\equiv\text{C-R})](\text{BF}_4)_x\}$ and μ_4 -dicarbide complexes $\{[(\mu\text{-PNNP})_2\{\text{Rh}(\text{CO})\}_4(\mu_4\text{-C}_2)](\text{BF}_4)_x\}$.

© 2011 Elsevier B.V. All rights reserved.

1. Introduction

Cooperative action of the plural metal centers in polynuclear species should lead to unique chemical behavior not observed for mononuclear species [1–9]. Our attention has been focused on reactivity of dinuclear complexes supported by PNNP-type quadridentate ligands. We first examined the dirhodium carbonyl complex with the 3,5-bis(diphenylphosphinomethyl)pyrazolato ligand (PNNP^{Py}; **A**) (Scheme 1) [10]. It has been revealed that, in the case of the corresponding dirhodium carbonyl complex **C**, the inner CO ligands are so labile owing to the influence of the P-donors *trans* to CO and the steric reason that the dicarbonyl species **D** with a *cis*-divacant site resulting from decarbonylation of **C** serves as an efficient 4e-acceptor to form the adduct **E** [11]. Later on we reported the complexes with the neutral 1,4-bis(diphenylphosphinomethyl)phthalazine ligand (PNNP^{Ph}; **B**) [12], which were studied to compare the characteristic features, i.e. the metal–metal separation and the charge. The shortened metal–metal separation ($l_3 < l_2$) frequently leads to *intraunit* metal–metal bond formation (see below), which has never been observed for the PNNP^{Py} system **A**.

Representative reaction behavior of the two $(\mu\text{-PNNP})\text{Rh}_2$ systems is summarized in Scheme 2 [11,12]. Carbonylation of the

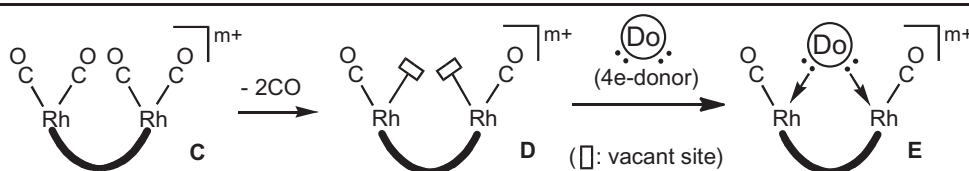
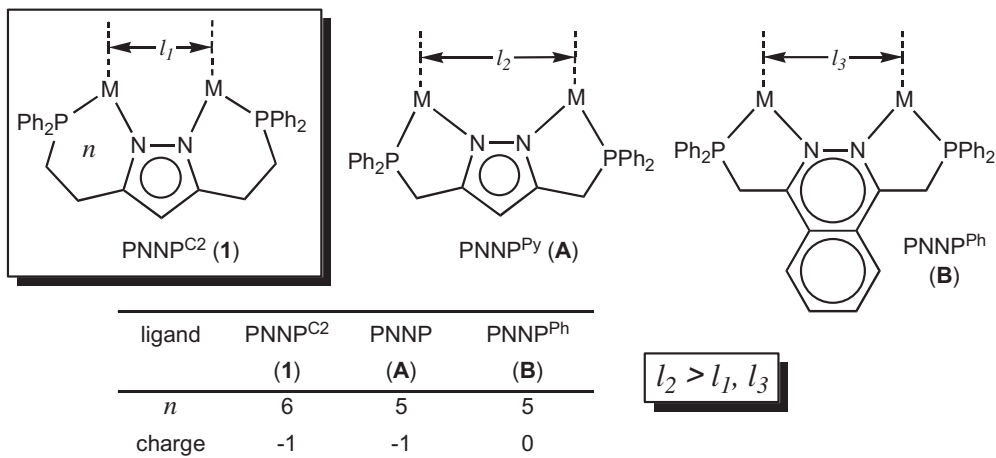
dirhodium-cod complex **E** affords the tetracarbonyl complex **C** (from **A**) and the dicarbonyl species **F** (from **B**). The two carbonyl species serve as an equivalent to the putative 4e-acceptor **D**; the tetracarbonyl species **C** loses the two inner carbonyl ligands to form **D** and the dicarbonyl species **F** with a formal Rh=Rh bond is an alternative canonical form of **D**. The dicarbonyl species **F** with the PNNP^{Ph} ligand (**B**) undergoes dimerization to form the tetrahedral tetrarhodium complex **G** with the *intraunit* Rh–Rh bonds in addition to the *interunit* Rh–Rh bonds. The coordinatively unsaturated species **D** serves as a 4e-acceptor. 1-Alkynes are incorporated, via deprotonation, into the dinuclear pocket as the bridging acetylide ligand (a 4e-donor) to form the dinuclear $\mu\text{-}\eta^1:\eta^2$ -acetylide complexes **H**, which show fluxional behavior as usually observed for this type of dinuclear species. The dinuclear adduct **H** further reacts with another coordinatively unsaturated species **D** to give the tetranuclear μ_4 -acetylide complex **I**, which shows dynamic behavior via reversible metal–metal bond scission and recombination processes and, in the case of the parent ethynyl complex (R=H), is converted to the μ_4 -dicarbide complex **J** upon deprotonation. In contrast to the formation of the bridging acetylide complexes commonly observed for the **A** and **B** systems including the tetranuclear adducts **I** with the unique structural features, reaction with internal alkyne depends on the ligand. Reaction with the PNNP^{Py} system (**A**) gives the simply $\mu\text{-}\eta^2:\eta^2$ -coordinated adduct **K**, whereas that of the PNNP^{Ph} system (**B**) results in oxidative addition to give the adduct **L**, in which the two

* Corresponding author.

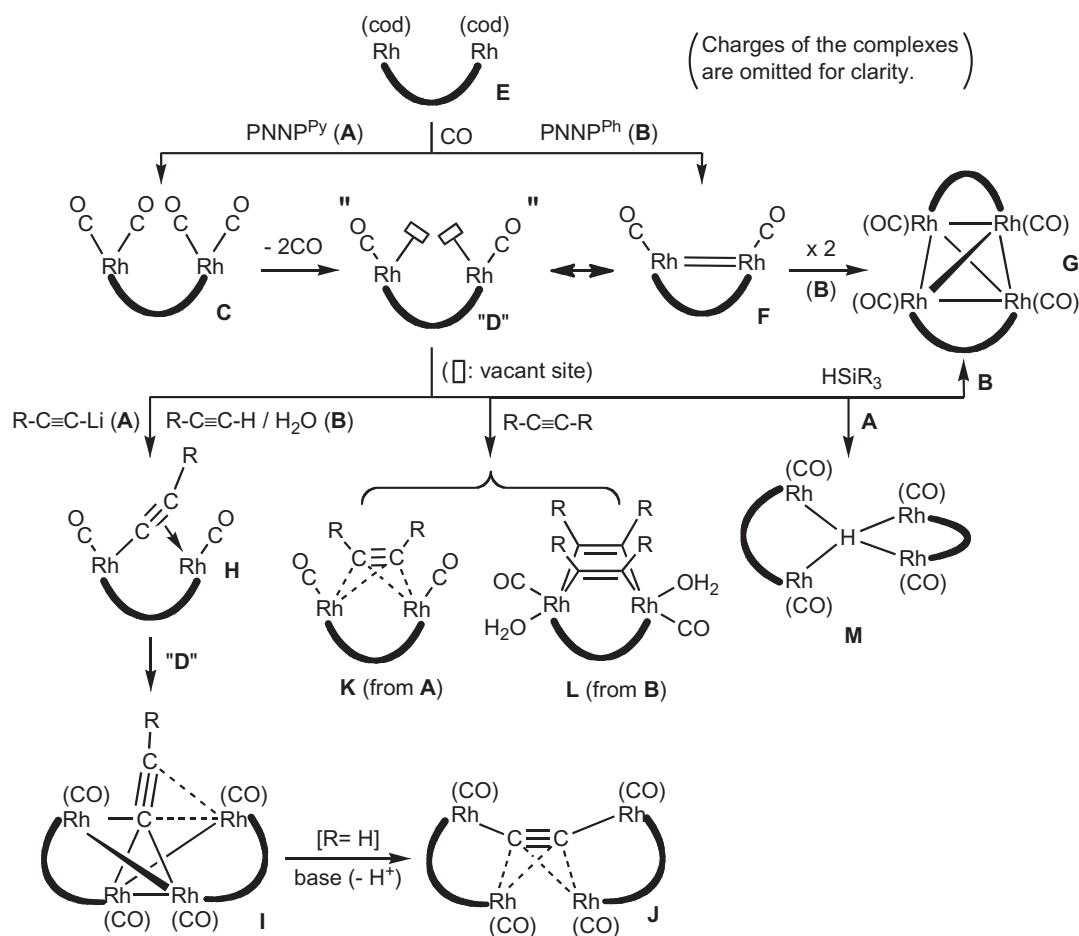
E-mail address: makita@res.titech.ac.jp (M. Akita).

alkyne molecules span the two metal centers to form the 1,3-dirhodacyclohexadiene skeleton. Dependence of the reaction pathway on the ligand is also observed for reaction with hydrosilane.

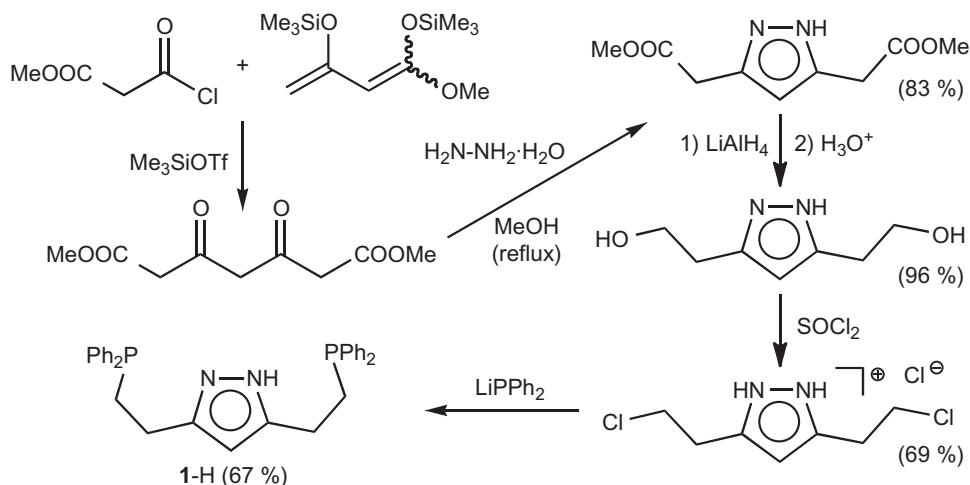
Reaction with the PNNP^{Py} species (A) affords the tetrahydridorhodium μ_4 -hydride complex M [11a,b], whereas that of the PNNP^{Ph} species (B) affords the tetrahydridorhodium product G without the hydride ligand.



Scheme 1.



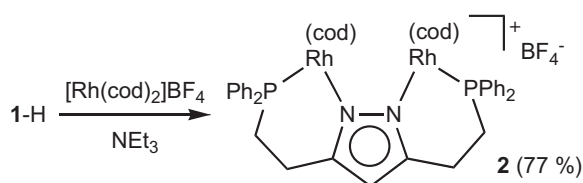
Scheme 2.



Scheme 3.

Although the appearance of the products look dissimilar, the formation of the two products has been interpreted in terms of the **M**-like intermediates $[(\mu\text{-PNNP})\text{Rh}_4(\text{CO})_4(\mu\text{-H})]^{n+}$ and has been ascribed to the different charge (n) of them. The charges of the **M**-like intermediates are +1 (**A**) and +2 (**B**), respectively. The more Lewis acidic dicationic intermediate with the PNNP^{Ph} ligands should undergo deprotonation to form the less positively charged monocationic species **G** $[(\mu\text{-PNNP}^{\text{Ph}})\text{Rh}_4(\text{CO})_4]^+$. Thus, while many reaction aspects of the two PNNP systems are similar, the different reactivity has been ascribed to the ring size as well as the charge of the intermediates.

In order to further examine the ring size and charge effects of the quadridentate ligands we have designed the diphenylphosphinoethyl analog of **A** (PNNP^{C2}; **1**) having (1) the six-membered metallacyclic moieties in place of the five-membered metallacyclic moieties in the PNNP^{Py} system and (2) –1 charge similar to the



Scheme 4.

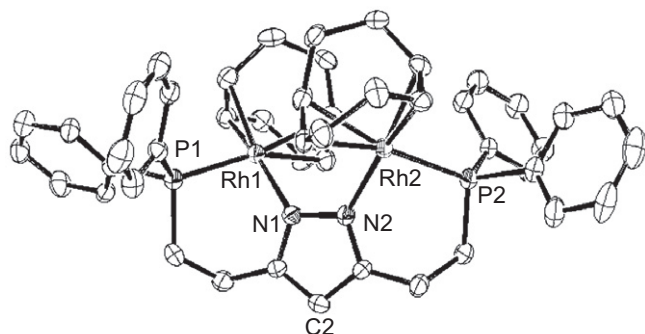


Fig. 1. An ORTEP view of the cationic part of **2** drawn with thermal ellipsoids at the 30% probability level. Only one of the two independent molecules with essentially the same coordination geometry is shown.

Table 1

Structural parameters for the dirhodium-cod complexes **2** and $[(\mu\text{-PNNP}^{\text{Ph}})\text{Rh}_2(\text{cod})_2](\text{BF}_4)_2$ **E(B)**.

2 ^a		E(B) ^b	
Molecule 1		Molecule 2	
<i>Bond lengths (Å)</i>			
Rh1...Rh2	4.1049(8)	Rh3...Rh4	4.1549(9)
Rh1–N1	2.091(6)	Rh3–N3	2.094(6)
Rh1–P1	2.320(3)	Rh3–P3	2.298(3)
Rh2–N2	2.096(7)	Rh4–N4	2.087(6)
Rh2–P2	2.298(2)	Rh4–P4	2.298(3)
Rh1–cod	2.139–	Rh3–cod	2.134–
	2.206(10)		2.235(12)
Rh2–cod	2.149–	Rh4–cod	2.150–
	2.244(9)		2.229(11)
<i>Bond angles and torsion angles (°)</i>			
N2–N1–Rh1	126.8(5)	N4–N3–Rh3	124.3(5)
N1–N2–Rh2	125.5(5)	N3–N4–Rh4	123.8(5)
N1–Rh1–P1	86.2(2)	N3–Rh3–P3	87.1(2)
N2–Rh2–P2	88.43(18)	N4–Rh4–P4	87.2(3)
Rh1–N1–N2–	47.4	Rh3–N3–N4–	63.7
Rh2		Rh4	

^a A unit cell of **2** contains two independent molecules with essentially the same geometry.

^b Relevant structural parameters. Ref. [12].

PNNP^{Py} system (Scheme 1). Herein we disclose (1) synthesis of the PNNP^{C2} ligand and its rhodium complexes and (2) reactions of the resultant dirhodium carbonyl species toward alkynes and HSiEt₃ furnishing unique adducts.

2. Results and discussion

2.1. Ligand synthesis

The PNNP^{C2} ligand precursor **1-H** was prepared following the synthetic route analogous to that of **A** (Scheme 3), which includes pyrazole ring construction [13] via condensation of 1,3-diketone with hydrazine. The 1,3-diketone precursor for **1**, dimethyl dioxopimelate [14], was prepared by acylation of 1-methoxy-1,3-bis(trimethylsilyloxy)butadiene [15] with methyl 3-chloro-3-oxopropionate catalyzed by trimethylsilyl triflate as reported by Chan [16]. The diketone was readily converted to 3,5-di(methoxycarbonylmethyl)pyrazole upon treatment with hydrazine hydrate.

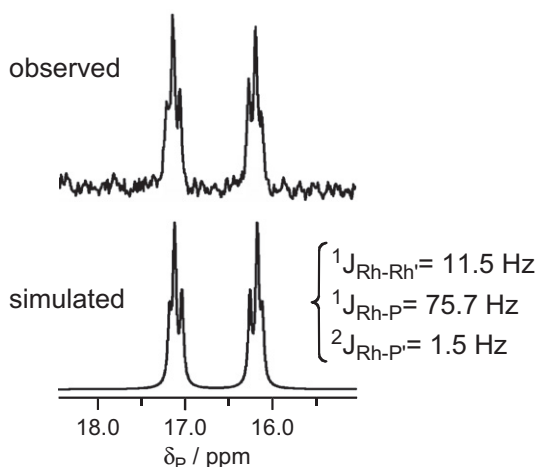
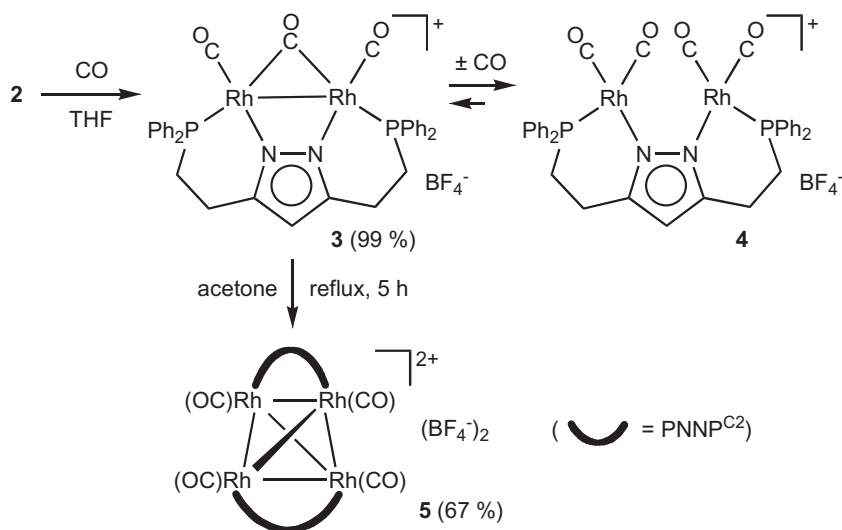


Fig. 2. Observed and simulated ^{31}P NMR spectra for **3** (observed at 122 MHz in acetone- d_6).

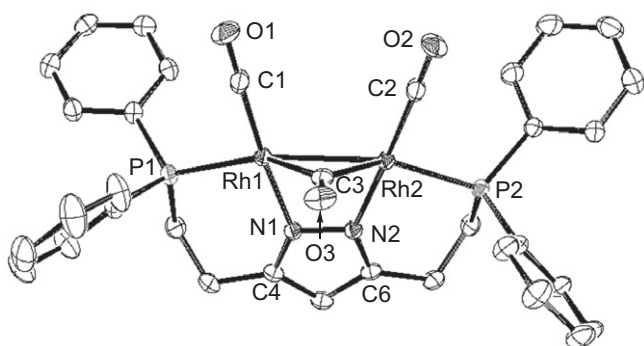


Fig. 3. An ORTEP view of the cationic part of **3** drawn with thermal ellipsoids at the 30% probability level.

Subsequent reduction with LiAlH_4 , chlorination with thionyl chloride and nucleophilic substitution with LiPPh_2 gave **1-H** as colorless solid. Ligand precursor **1-H** is readily characterized on the basis of its spectroscopic data ($\delta_{\text{P}} -15.3$; for other data, see experimental part), which supports the symmetrical structure.

2.2. Preparation of cod complex **2**

Reaction of the obtained $\text{PNNP}^{\text{C}2}$ ligand precursor **1-H** with the labile cod complex of rhodium, $[\text{Rh}(\text{cod})_2]\text{BF}_4$, in CH_2Cl_2 readily afforded the cationic 1: 2 adduct **2**, $[(\mu\text{-}\kappa^2\text{:}\kappa^2\text{-PNNP}^{\text{C}2})\{\text{Rh}(\eta^2\text{:}\eta^2\text{-cod})\}_2]\text{BF}_4$, as yellow crystals (Scheme 4). The composition and symmetrical structure of the products are confirmed by the single sets of NMR signals for the $\text{CH}_2\text{CH}_2\text{P}$, and cod parts, and P-coordination is verified by the doublet ^{31}P NMR signal ($\delta_{\text{P}} 23.5$ (d, $J_{\text{P-Rh}} = 150.4$ Hz)) resulting from coupling with a Rh nucleus. The $^1J_{\text{Rh-P}}$ value for **2** is comparable to those of the PNNP^{Ph} complex (**E(B)**; $\delta_{\text{P}} 28.0$ (d, $J_{\text{P-Rh}} = 148.4$ Hz)) and the PNNP^{Py} complex (**E(A)**; $\delta_{\text{P}} 41.6$ (d, $J_{\text{P-Rh}} = 154.5$ Hz)¹).

The cod complex **2** is also characterized by X-ray crystallography (Fig. 1 and Table 1). A unit cell contains two independent molecules with essentially the same geometry. The structural characterization reveals (1) square-planar geometry of the metal centers coordinated by the bridging $\mu\text{-}\kappa^2\text{:}\kappa^2\text{-PNNP}^{\text{C}2}$ ligand and the $\eta^2\text{:}\eta^2\text{-cod}$ ligand, (2) a twisted C_2 -symmetry-like structure with respect to the axis passing through the C2 atom and the midpoint of the N1–N2 bond, which is caused by steric repulsion between the bulky $\text{Rh}(\text{cod})$ fragments as is indicated by the large $\langle \text{Rh1-N1-N2-Rh2} \rangle$ dihedral angles ($47.4(9)^\circ$ and $63.7(8)^\circ$), (3) $\text{Rh}\cdots\text{Rh}$ separations ($4.1049(8)$ Å and $4.1549(9)$ Å) being substantially longer than the sum of covalent radius (2.68 Å), and (4) the pseudo-chair conformation of the six-membered chelate rings. Comparison with the PNNP^{Ph} derivative **E(B)** (Table 1) reveals the following features: (1) the bond lengths are comparable, (2) the N–Rh–P bond angles of **2** closer to the right angle and larger than that of **E(B)** by ca. 10° indicate lesser distortion from ideal square-planar coordination geometry, and (3) the $\text{Rh}\cdots\text{Rh}$ separation and the Rh–N–N–Rh dihedral angle for **2** are slightly larger than those of **E(B)**. Although incorporation of the two six-membered chelate rings in **2** (vs. one six-membered ring in **E(B)**) may cause shortening of the $\text{Rh}\cdots\text{Rh}$ separation, this is not the case (feature 3). The elongation of the $\text{Rh}\cdots\text{Rh}$ separation of **2** may be interpreted in terms of the more severe steric repulsion between the bulky $\text{Rh}(\text{cod})$ fragments in **2**, which are brought closer by the introduction of the two six-membered metallacyclic ring structures.

¹ The abbreviation **X(Y)** stands for the X-type complex with the Y ligand.

2.3. Carbonylation of cod complex **2**: formation of tricarbonyl species **3** and its interconversion with carbonyl species with a more and lesser number of CO ligands

Carbonylation of **2** in CH₂Cl₂ at room temperature gave the orange product **3** in a quantitative yield. (Scheme 5). Single sets of NMR signals for the PNNP^{C2} part indicating a symmetrical structure and the IR band for a bridging CO ligand (1897 cm⁻¹; ν(η¹-CO) 2052, 1986 cm⁻¹) lead to formulation of the product **3** as

$[(\mu-\kappa^2:\kappa^2\text{-PNNP}^{\text{C2}})\text{Rh}_2(\text{CO})_2(\mu\text{-CO})]\text{BF}_4$. The presence of a Rh–Rh bond is also supported by the $^1J_{\text{Rh-Rh}}$ coupling, which must be taken into account for successful analysis of the multiplet ^{31}P NMR signals (Fig. 2). In the previous paper [12] we reported that $^1J_{\text{Rh-Rh}}$ coupling is a diagnostic for a Rh–Rh bonding interaction.

Molecular structure of **3** determined by X-ray crystallography (Fig. 3 and Table 2) is consistent with the structure proposed on the basis of the spectroscopic data. The Rh₂N₂P₂ moiety is virtually planar as is evident from the very small values of the relevant

Table 2
Selected structural parameters for **3**^a

Bond lengths (Å)		Bond angles (°)			
Rh1–Rh2	2.7091(6)	Rh2–Rh1–P1	157.13(4)	Rh1–Rh2–C3	48.15(15)
Rh1–P1	2.3135(16)	Rh2–Rh1–N1	70.84(13)	P2–Rh2–N2	87.69(13)
Rh1–N1	2.029(4)	Rh2–Rh1–C1	105.5(2)	P2–Rh2–C2	93.32(18)
Rh1–C1	1.859(6)	Rh2–Rh1–C3	47.75(14)	P2–Rh2–C3	141.06(14)
Rh1–C3	2.029(5)	P1–Rh1–N1	88.73(13)	N2–Rh2–C2	176.31(19)
Rh2–P2	2.3007(13)	P1–Rh1–C1	93.8(2)	N2–Rh2–C3	90.31(19)
Rh2–N2	2.033(5)	P1–Rh1–C3	144.95(16)	C2–Rh2–C3	91.1(3)
Rh2–C2	1.879(6)	N1–Rh1–C1	173.6(2)	N–1–N2–C6	108.8(5)
Rh2–C3	2.016(5)	N1–Rh1–C3	88.36(18)	Rh1–C1–O1	179.3(6)
P1–C8	1.813(6)	C1–Rh1–C3	92.9(3)	Rh2–C2–O2	179.4(5)
O1–C1	1.151(7)	Rh1–Rh2–P2	157.36(4)	Rh1–C3–Rh2	84.10(18)
O2–C2	1.133(8)	Rh1–Rh2–N2	70.42(12)	Rh1–C3–O3	137.1(5)
O3–C3	1.146(6)	Rh1–Rh2–C2	108.18(18)	Rh2–C3–O3	138.2(5)

^a Dihedral angles: (Rh1–N1–N2–Rh2) = 6.2°, (C4–N1–Rh1–P1) = 8.0°, (C6–N2–Rh2–P2) = 2.4°.

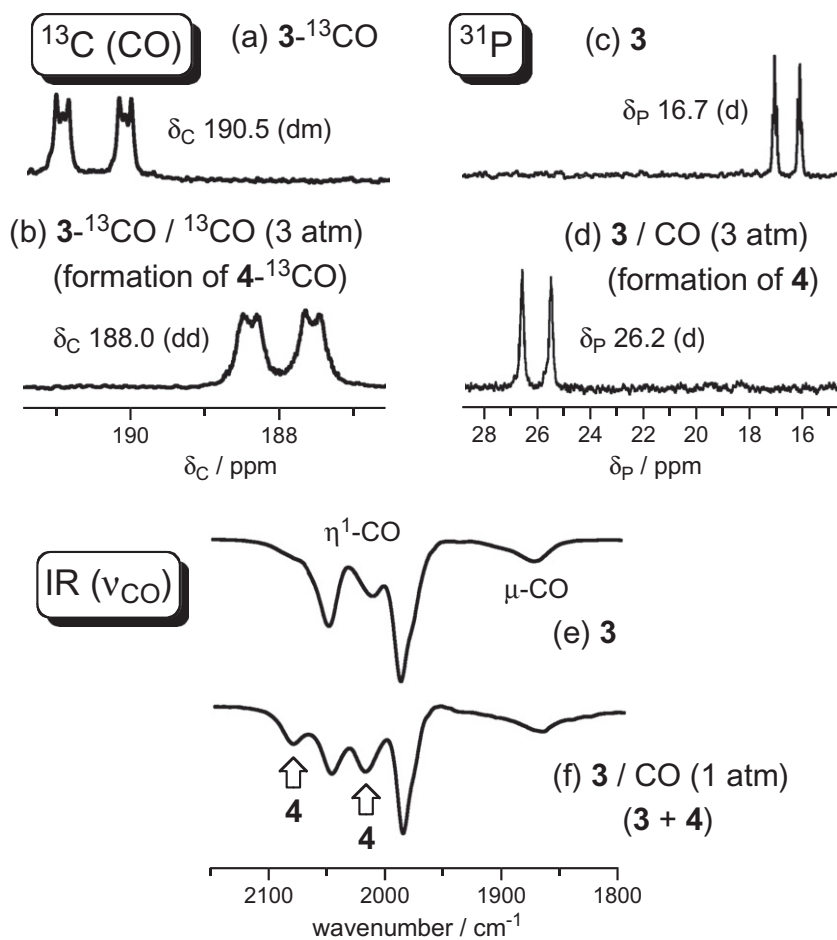
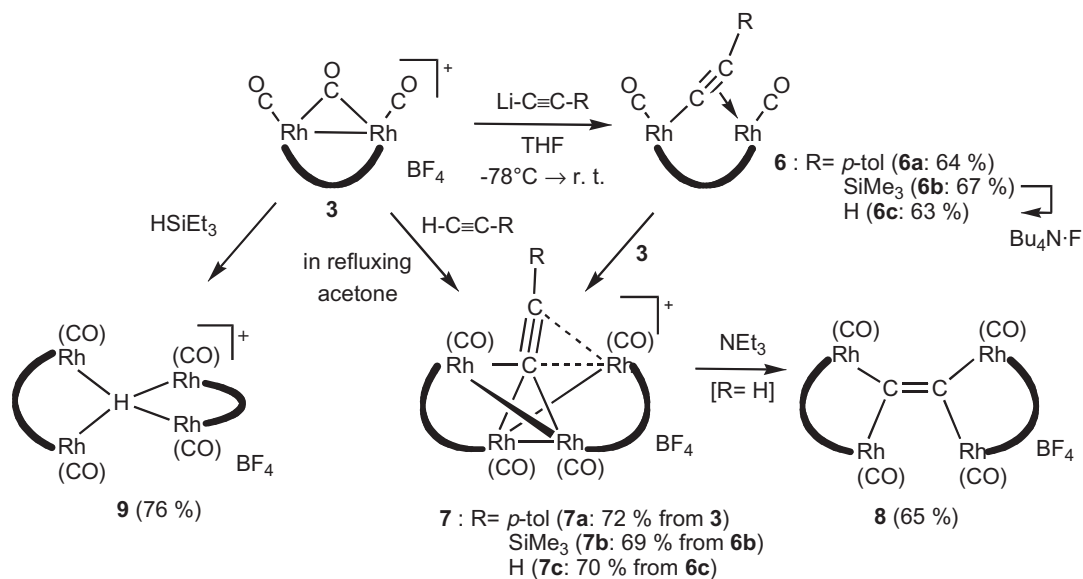


Fig. 4. Spectral changes of **3** observed under CO atmosphere (NMR and IR spectra were recorded in acetone-*d*₆ and THF, respectively). ^{31}P and ^{13}C NMR spectra were observed at 122 MHz and 75 MHz, respectively): (a) A ^{13}C NMR spectrum of ^{13}C -enriched **3** ($^3\text{-}^{13}\text{CO}$). (b) A ^{13}C NMR spectrum of $^3\text{-}^{13}\text{CO}$ observed under ^{13}CO (3 atm). (c) A ^{31}P NMR spectrum of **3**. (d) A ^{31}P NMR spectrum of **3** observed under CO (3 atm). (e) An IR spectrum of **3**. (f) An IR spectrum of **3** observed under CO (1 atm).



Scheme 6.

dihedral angles shown in Table 2. The terminal and bridging CO ligands are located virtually in-plane and perpendicular with respect to the Rh₂N₂P₂ coordination plane, respectively, and the core structure turns out to be isostructural with that of the Ir-PNNP^{Ph} derivative, [μ-PNNP^{Ph}Ir₂(CO)₂(μ-CO)](BF₄)₂, reported by us previously [12].

It is notable that the number of the carbonyl ligands (*n*) of the dirhodium carbonyl species of the three PNNP systems, [(μ-PNNP)Rh₂(CO)_{*n*}](BF₄)_{*x*}, in other words, the structures of the carbonyl species, are dependent on the quadridentate ligand: *n* = 2 (PNNP^{Ph}: **F**), 3 (PNNP^{C2}: **3**), 4 (PNNP^{Pv}: **C(A)**). The results could be interpreted in terms of the metal–metal distance as well as the charge. For the PNNP^{Pv} complex **C(A)**, the two metal centers are too much separated to interact with each other, whereas, for the PNNP^{Ph} complex **F**, the metal–metal distance is short enough for bond formation but the metal centers can carry a lesser number of CO ligands because of the weaker back-donation from the more positively charged metal centers. In the case of the PNNP^{C2} complex **3**, the shorter metal–metal separation and the efficient back-donation from the less positively charged metal centers should cause formation of the metal–metal bonded species with a bridging CO ligand. The tricarbonyl species **3** is a 32 valence electron species, which is electron-precise as a dinuclear species with a metal–metal single bond.

The flexibility of the number of the CO ligand in the PNNP–Rh₂ system prompted us to examine interconversion of **3** with species with a more or lesser number of the CO ligands via carbonylation or decarbonylation, respectively. First of all, occurrence of inter- and intra-molecular exchange reactions of the CO ligands is verified by the ¹³C NMR experiments: (1) intermolecular process: Pressurization of **3** with ¹³CO (3 atm) followed by ¹³C NMR measurement under N₂ (1 atm) revealed ¹³C-enrichment of the CO signals of **3** indicating incorporation of external ¹³CO molecules (Fig. 4a). (2) intramolecular process: A ¹³CO-enriched sample (**3**-¹³CO) showed a single δ_C(CO) signal (δ_C 190.5 (dm, ¹J_{Rh–C} = 63.2 Hz)² indicative of η¹–μ site exchange processes of the CO ligands occurring at a rate faster than the NMR timescale (Fig. 4a).

A ¹³C NMR spectrum of **3**-¹³CO observed under ¹³CO atmosphere (3 atm) (Fig. 4b) showed formation of a new species (δ_C 188.0 (dd, ¹J_{Rh–C} = 62.3 Hz, ²J_{P–C} = 14.2 Hz)) assignable to the tetracarbonyl species **4** (Scheme 5). ³¹P NMR measurement of **3** under CO atmosphere (3 atm) also revealed complete conversion to a new species (δ_P 25.0 (¹J_{Rh–P} = 126.0 Hz)) (Fig. 4c and d). The lack of a ¹J_{Rh–Rh} coupling suggests disruption of the Rh–Rh bond in **3** [12]. IR measurement of **3** under CO atmosphere (1 atm) further confirmed formation of a new species showing CO vibrations at 2081 and 2021 cm⁻¹ (Fig. 4e and f). (Because the IR measurement was carried out under 1 atm, conversion to the new species was incomplete.) These spectroscopic behavior is consistent with inter-conversion between the metal–metal bonded tricarbonyl species **3** and the non-metal–metal bonded tetracarbonyl species **4** (Scheme 5), and the tetracarbonyl species **4** is stable only under CO pressure.

On the other hand, refluxing an acetone solution of **3** furnished the dark red product **5** (Scheme 5). Although crystallographic data is not available, the spectroscopic data for **5** comparable to those of **G** suggest formation of an analogous symmetrical tetrahedral species of the formula of [(PNNP^{C2})₂Rh₂(CO)₄](BF₄) as supported by the ESI-MS data and the single CO vibration. The metal–metal bond formation is supported by the ¹J_{Rh–Rh} coupling taken into account on simulation of the ³¹P NMR signal. The tetrahedral species **5** should be formed by dimerization of the dicarbonyl species **D(1)** resulting from thermal decarbonylation of **3**.

2.4. Reaction of CO complex **3** with lithium acetylide, 1-alkyne and HSiEt₃

In order to compare the reactivity of the PNNP^{C2} complex **3** it was subjected to reaction with lithium acetylide, 1-alkyne, and HSiEt₃, the reactivity of which toward the PNNP^{Pv} and PNNP^{Ph} complexes was already studied (Scheme 2). The reaction products were characterized by comparison of their spectroscopic features with those of the PNNP^{Pv} derivatives.

2.4.1. With lithium acetylide and 1-alkyne

The reactivity of the PNNP^{C2} complex **3** (Scheme 6) turned out to be essentially the same as that of the PNNP^{Pv} complex **D(A)** (Scheme 2). Reaction with lithium acetylide gave the dinuclear

² The multiplet signals should result from coupling with the η¹- and μ-¹³CO ligands.

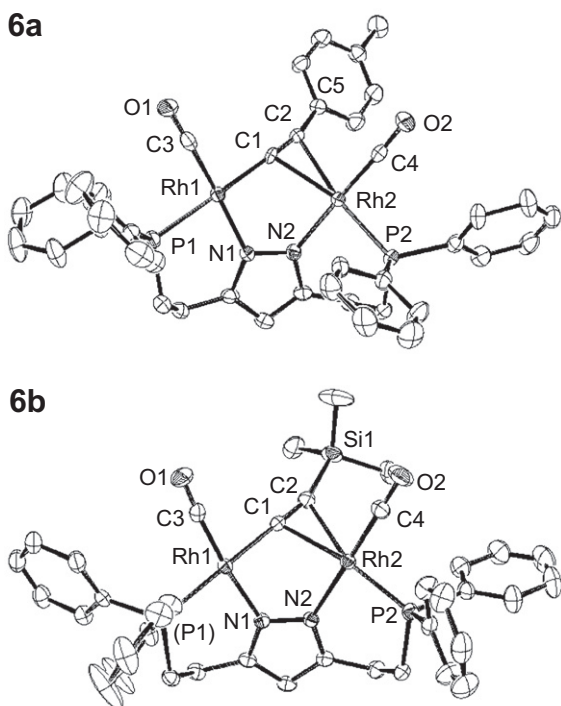


Fig. 5. ORTEP views of **6a** and **6b** drawn with thermal ellipsoids at the 30% probability level.

μ - η^1 : η^2 -acetylide complex **6**. Subsequent treatment of the resultant complex **6** with **3** afforded the tetranuclear μ_4 -acetylide

complex **7**, which was also obtained by direct treatment of **3** with 1-alkyne. Refluxing in acetone was needed for the formation of **7**, while the reaction of the PNNP^{Py} system proceeded at room temperature. The more harsh conditions may be required for removal of the bridging ligand. Deprotonation of the $C\equiv C-H$ complex **7c** gave the μ_4 -dicarbide complex **8** (Scheme 6) in a manner similar to the PNNP^{Py} system (**J**; Scheme 2). The dinuclear μ -acetylide complexes **6** were characterized by spectroscopic and crystallographic methods, while the tetranuclear species **7** and **8** were characterized spectroscopically, in particular, on the basis of their NMR features (1:2 adducts) and ESI-MS data, as also compared with the corresponding PNNP^{Py} derivatives (see experimental section). Complexes **6–8** showed dynamic behavior as observed for the PNNP^{Py} and PPNP^{Ph} complexes **H–J** (Scheme 2).

The dinuclear μ -acetylide complexes **6a** and **6b** are characterized by X-ray crystallography (Fig. 5 and Table 3). When the two PNNP^{C2}-acetylide complexes **6a** and **6b** with essentially the same core geometry are compared, it is revealed that (1) the Rh...Rh separations are between those for the metal–metal bonded species **3** and the non-metal–metal bonded species **2** and (2) the steric repulsion between the Rh fragments is released significantly when compared with **2** as is evident from the Rh–N–N–Rh torsion angles.

For comparison of the coordination properties provided by the three PNNP ligands selected structural parameters for the *p*-tolylethynyl complexes with the PNNP^{C2} (**6a**), PNNP^{Py} (**H(A)**) and PNNP^{Ph} ligands (**H(B)**) are listed in Table 3. Incorporation of the six-membered ring structure(s) into the central tricyclic chelate-heterocycle-chelate moiety in **6a** and **H(B)** causes shortening of the Rh...Rh distance when compared to the PNNP^{Py} complex **H(A)** but the effect is saturated as can be seen from the distances for **6a** and **H(B)**. The shortening brings about the dissymmetric

Table 3

Comparison of structural parameters for the dirhodium μ -acetylide complexes, $[(\mu-L)Rh_2(CO)_2(\mu-C\equiv C-R)](BF_4)_n$ ($R/L = p\text{-tol/PNNP}^{C2}$ (**6a**), $SiMe_3/PNNP^{C2}$ (**H(A)**), $p\text{-tol/PNNP}^{Py}$ (**H(A)**), and $p\text{-tol/PNNP}^{Ph}$ (**H(B)**)).

Complex	6b PNNP ^{C2} /SiMe ₃ 6-5-6/0	6a PNNP ^{C2} / <i>p</i> -tol 6-5-6/0	H(B) ^a PNNP ^{Ph} / <i>p</i> -tol 5-6-5/1	H(A) ^b PNNP ^{Py} / <i>p</i> -tol 5-5-5/0
<i>Interatomic distances (Å)</i>				
Rh1...Rh2	3.3882(4)	3.4475(7)	3.341(1)	3.6169(4)
C1–C2	1.224(5)	1.216(8)	1.23(2)	1.205(5)
Rh1–C1	2.008(3)	2.050(6)	2.001(1)	2.061(3)
Rh2–C1	2.279(3)	2.273(6)	2.25(1)	2.338(2)
Rh2–C2	2.387(4)	2.364(6)	2.39(1)	2.338(3)
Rh1–P1	2.2985(9)	2.2688(16)	2.270(3)	2.2768(3)
Rh1–N1	2.055(3)	2.063(5)	2.106(2)	2.030(7)
Rh1–C3	1.817(4)	1.830(7)	1.80(1)	1.826(3)
Rh2–P2	2.2533(9)	2.2637(17)	2.226(3)	2.2405(7)
Rh2–N2	2.077(3)	2.062(6)	2.119(7)	2.066(2)
Rh2–C4	1.809(4)	1.802(7)	1.80(1)	1.825(3)
Δ	0.108	0.091	0.14	0.000
<i>Bond angles and torsion angles (°)</i>				
C1–C2–X	161.7(3) (Si1) ^d	167.1(6) (C5) ^d	169(1)	164.3(3)
Rh1–C1–Rh2	104.24(13)	105.6(3)	103.6(4)	110.5(1)
Rh1–C1–C2	171.5(3)	167.7(5)	169.7(8)	168.7(3)
Rh2–C1–C2	79.7(2)	79.0(4)	80.8(7)	77.5(2)
C1–Rh2–C2	30.31(11)	30.3(2)	30.6(4)	29.5(1)
P1–Rh1–N1	90.43(7)	90.62(15)	80.2(2)	80.07(8)
P1–Rh1–C3	94.19(10)	87.0(2)	96.6(4)	99.1(1)
N1–Rh1–C1	85.66(11)	87.3(3)	90.3(4)	88.2(1)
P2–Rh2–N2	89.23(7)	86.93(15)	79.9(2)	77.89(6)
P2–Rh2–C4	90.23(12)	90.7(3)	90.9(4)	93.15(9)
N2–Rh2–C1	81.50(11)	81.6(2)	84.7(3)	82.55(9)
Rh1–N1–N2–Rh2	2.5	12.7	6.3	1.0
X–N1–Rh1–P1	28.8 (C8) ^d	15.8 (C14) ^d	22.4	3.8
X–N2–Rh2–P2	33.3 (C10) ^d	35.5 (C12) ^d	22.3	11.3

^a Ref. [12].

^b Ref. [11d].

^c The three digits refer to the ring sizes of the chelate–bridging heterocycle–chelate part.

^d X.

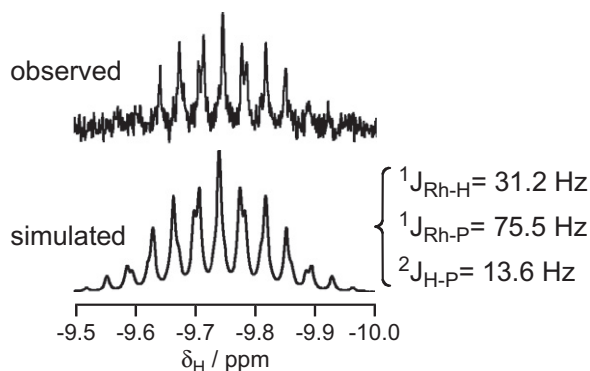


Fig. 6. Observed and simulated ^1H NMR spectra (hydride region) for **9** (observed at 400 MHz in acetone- d_6).

η^2 -coordination of the $\text{C}\equiv\text{C}$ part as can be seen from the differences of the C1–Rh2 and C2–Rh2 distances (Δ ; Table 3). Strain caused by the dissymmetric coordination may be partly released by puckering of the flexible chelate rings as is evident from the X–N1–Rh1–P1 and X–N2–Rh2–P2 torsion angles substantially larger than those for **H(A)**.

2.4.2. With HSiEt_3

Reaction of **3** with HSiEt_3 afforded the purple μ_4 -hydride complex **9** in a manner similar to the reaction of **D(A)** (Scheme 6) [11a,b]. The formation of **9** has been confirmed by the ESI-MS data and ^1H NMR simulation of the multiplet hydride signal, which has been successfully analyzed by taking into account coupling with the four equivalent Rh–P moieties (Fig. 6).

2.5. Coordination features of $\text{PNNP}^{\text{C}2}$ ligand (**1**) as compared with PNNP^{P^y} (**A**) and PNNP^{P^h} ligands (**B**)

The following conclusion can be deduced from the obtained results.

Many similarities in the reactivity of the dirhodium-carbonyl species **3**, **C(A)** and **C(B)** have been noted not only for the conventional species such as the dinuclear μ -acetylide complexes (**6**, **H(A)**, and **H(B)**) but also for the unique, tetranuclear μ_4 -acetylide cluster compounds (**7**, **I(A)**, and **I(B)**) and μ_4 -dicarbide complexes (**8**, **J(A)**, and **J(B)**). The present study reveals that the PNNP ligand set provides a scaffold for such unique structures, which have never been observed for other ligand systems.

Meanwhile, following dissimilarities are also noted.

- (1) *Ring size effect*: Incorporation of the enlarged six-membered ring(s) into the chelate-heterocycle-chelate moiety (**1** and **B**) causes shortening of the metal–metal distance, which frequently leads to the *intra-unit* M–M bond formation as exemplified by **5** and **G(B)**.
- (2) *Charge effect*: The coordination properties of the complexes derived from the two mononegative ligands (**1** and **A**) turn out to be the very similar, while they differ from those derived from the neutral ligand (**B**) to a considerable extent.
- (3) *The different numbers of the carbonyl ligands in the carbonyl complexes*: This aspect has been interpreted in terms of a combination of the two factors mentioned above. In the case of the $\text{PNNP}^{\text{C}2}$ complex **2**, the shortening of the metal–metal distance and the effective back donation from the monocationic (PNNP)Rh $_2$ fragment lead to the formation of the carbonyl species **2** with a Rh–Rh single bond as well as three bridging CO ligands, one of which spans the two metal centers in a bridging mode.

3. Experimental

3.1. General methods

All manipulations were carried out under an inert atmosphere by using standard Schlenk tube techniques. THF, ether, hexane (Na–K alloy), CH_2Cl_2 (P_2O_5), acetone (CaH_2), and ROH ($\text{Mg}(\text{OR})_2$; R=Me, Et) were treated with appropriate drying agents, distilled, and stored under argon. Because analytically pure samples of the products could not be obtained despite several attempts, they were characterized by spectroscopic methods and, for some cases, crystallographic method as well. ^1H and ^{31}P NMR spectra were recorded on Bruker AC-200 (^1H , 200 MHz; ^{31}P , 81 MHz) and JEOL JMN-EX-300 spectrometers (^1H , 300 MHz; ^{13}C , 75 MHz; ^{31}P , 122 MHz). Chemical shifts are reported in ppm downfield from TMS (^1H and ^{13}C) and H_3PO_4 (^{31}P) and coupling constants are reported in Hz. Solvents for NMR measurements containing 0.5% TMS were dried over molecular sieves, degassed, distilled under reduced pressure, and stored under Ar. IR spectra were obtained on a JASCO FT/IR 5300 spectrometer. ESI-MS spectra were recorded on a ThermoQuest Finnigan LCQ Duo mass spectrometer. The procedures for X-ray crystallographic analysis were similar to those reported in our previous paper, with the exception of the use of CrystalStructure ver. 4.0 in place of teXsan [17]. 1-Methoxy-1,3-bis(trimethylsiloxy)butadiene [15] and $[\text{Rh}(\text{cod})_2]\text{BF}_4$ [10a] were prepared according to the published procedures. Other chemicals were purchased and used as received.

3.2. Preparation of 3,5-bis(diphenylphosphinoethyl)pyrazole (**1-H**)

3,5-Di(methoxycarbonylmethyl)pyrazole: To a MeOH solution of dimethyl dioxopimelate [14] (3.31 g, 15.3 mmol) was added hydrazine hydrate (1.6 mL, 32 mmol), and the resultant mixture was refluxed for 1 h. After removal of the volatiles the resultant yellow residue was extracted with ethyl acetate (200 mL). Evaporation of the volatiles gave the product as dark brown oil, which was used without further purification. 3,5-Di(methoxycarbonylmethyl)pyrazole (3.13 g, 12.7 mmol, 83% yield): δ_{H} (CDCl_3) 6.14 (1H, s, pyrazole ring proton), 3.71 (10H, s (overlapped), $\text{CH}_2 + \text{OMe}$).

3,5-Di(2-hydroxyethyl)pyrazole: To a THF suspension (50 mL) of LiAlH_4 (1.83 g, 48.1 mmol) was added a THF solution (150 mL) of 3,5-di(methoxycarbonylmethyl)pyrazole (3.13 g, 12.7 mmol) dropwise at room temperature. After being stirred for 30 min at the same temperature, the reaction mixture was refluxed for 10 h. The resultant mixture was carefully hydrolyzed with water (30 mL) and then the volatiles were removed under reduced pressure. The obtained residue suspended in MeOH (200 mL) was bubbled with CO_2 for 10 min and refluxed for 8 h. Filtration through a Celite pad followed by evaporation gave the product as brown oil (2.22 g, 14.2 mmol, 96% yield). 3,5-Di(2-hydroxyethyl)pyrazole: δ_{H} (CDCl_3) 5.95 (1H, s, pyrazole ring proton), 3.91 (4H, t, $J = 5.5$ Hz, CH_2OH), 2.87 (4H, t, $J = 5.5$ Hz, $\text{CH}_2\text{CH}_2\text{OH}$).

3,5-Di(chloroethyl)pyrazolium chloride: 3,5-di(2-hydroxyethyl)pyrazole (2.66 g, 17.0 mmol) was dissolved in SOCl_2 (25 mL) and refluxed for 30 min. After removal of the volatiles under reduced pressure the residue was extracted with EtOH and filter through a Celite plug. Evaporation of the solvent gave the product as dark brown oil (3.19 g, 11.7 mmol, 69% yield). 3,5-Di(chloroethyl)pyrazolium chloride: δ_{H} (CDCl_3) 6.46 (1H, s, pyrazole ring proton), 3.88 (4H, t, $J = 6.2$ Hz, CH_2Cl), 3.34 (4H, t, $J = 6.2$ Hz, $\text{CH}_2\text{CH}_2\text{Cl}$).

3,5-Bis(diphenylphosphinoethyl)pyrazole (1-H**)**: To a THF solution (15 mL) of PPh_3 (4.38 g, 16.7 mmol) was added Li wire (241 mg, 34.7 mmol), and the resultant mixture was stirred for 3 h at room temperature. To the resultant solution of LiPPh_2 cooled at -78°C

was added 3,5-di(chloroethyl)pyrazolium chloride (952 mg, 4.15 mmol), and the mixture was stirred for 2 h at 0 °C and then for 30 min at room temperature. Deaerated water was added to destroy the excess LiPPh₂. Extraction with ether, drying over Na₂SO₄, and filtration, and removal of the volatiles under reduced pressure left pale yellow solid, which was dissolved in ether (2 mL) and chromatographed on silica gel under inert atmosphere (eluted with ether/hexane (1: 1) → ether) to give **1-H** as colorless solid (1.37 g, 2.78 mmol, 67% yield). **1-H**: δ_H (CDCl₃) 7.4–7.3 (20H, m, Ph), 5.90 (1H, s, pyrazole ring proton), 2.69 (4H, t, J = 8.5 Hz, CH₂P), 2.36 (4H, t, J = 8.5 Hz, CH₂CH₂P). δ_P (CDCl₃) –15.3.

3.3. Preparation of [(μ-PNNP^{C2}){Rh(cod)}₂]BF₄ (**2**)

To a CH₂Cl₂ solution (15 mL) of [Rh(cod)₂]BF₄ (1.01 g, 2.49 mmol) was added **1** (604 mg, 1.23 mmol) dissolved in CH₂Cl₂ (15 mL). After the mixture was stirred for 2 min NEt₃ (0.17 mL, 1.23 mmol) was added. The mixture was further stirred for 30 min at room temperature. The organic phase was washed with deaerated water three times and dried over Na₂SO₄. Filtration, evaporation and crystallization of the residue from THF/ether gave **2** as yellow crystals (951 mg, 0.95 mmol, 75% yield). **2**: δ_H (CDCl₃) 8.0–6.8 (20H, m, Ph), 6.00 (1H, s, pyrazole ring proton), 3.9–3.7, 3.5–3.3, 3.0–2.8, 2.7–2.4, 2.25–1.95, 1.95–1.85, 1.85–1.5 (32H, m, cod + CH₂CH₂). δ_P (CDCl₃) 23.5 (d, J = 151 Hz).

3.4. Preparation of [(μ-PNNP^{C2})Rh₂(CO)₃]BF₄ (**3**)

CO gas was bubbled through a THF suspension (10 mL) of **1** (286 mg, 0.285 mmol) for 1 h. Removal of the volatiles under reduced pressure and crystallization of the residue from THF/ether gave **3** as orange crystals (240 mg, 0.276 mmol, 97% yield). **3**: δ_H (CDCl₃) 7.9–7.7 (20H, m, Ph), 6.00 (1H, s, pyrazole ring proton), 2.99, 2.83 (4H × 2, br × 2, CH₂CH₂); δ_P (CDCl₃) 16.7 (d, J = 153 Hz); IR (KBr) 2063, 2040, 1897 cm⁻¹; ESI-MS: m/z = 781 (M⁺ for the cationic part).

3.5. Carbonylation of **3** leading to tetracarbonyl species [(μ-PNNP^{C2})Rh₂(CO)₄]BF₄ (**4**)

An acetone-*d*₆ solution of **3** was prepared in a thick-walled pressure NMR tube equipped with a rubber septum, which was then capped. CO or ¹³CO was injected through the rubber septum on the top via a gastight syringe. In the case of the measurements under 3 atm of CO or ¹³CO, the amount of the injected gas was calculated on the basis of the volume of the NMR tube.

3.6. Thermolysis of **3** giving tetrarhodium complex [(μ-PNNP^{C2})₂Rh₄(CO)₄](BF₄) (**5**)

Refluxing an acetone solution of **3** for 5 h followed by precipitation with hexane gave black solid **5** (62% yield). **5**: δ_H (acetone-*d*₆) 2.55–4.20 (16H, m), 6.70 (2H, s, pz), 7.1–8.0 (40H, m, Ph); δ_P (acetone-*d*₆) 25.7 (¹J_{Rh-P} = 140.0 Hz, ¹J_{Rh-Rh} = 16.0 Hz, ²J_{Rh-P} = 6.0 Hz; δ_C (acetone-*d*₆) 192.0 (dd, ¹J_{Rh-C} = 66.1 Hz, ²J_{P-C} = 12.3 Hz; IR (KBr) 2008 cm⁻¹; ESI-MS m/z = 1450.8 ([PNNP^{C2}]₂Rh₂(CO)₂]⁺; M⁺ – 2CO), 1421.9 ([PNNP^{C2}]₂Rh₂(CO)]⁺; M⁺ – 3CO), 753.3 ([PNNP^{C2}]₂Rh₂(CO)₄]²⁺; M²⁺)

3.7. Preparation of [(μ-PNNP^{C2}){Rh(CO)}₂(μ-C≡C-R)]BF₄ (**6**)

p-Tol derivative (**6a**): LiC≡C-*p*-tol was generated by treatment of a THF solution (5 mL) of H-C≡C-*p*-tol (40 μL, 0.302 mmol) with *n*-BuLi (1.54 M, 0.18 mL, 0.277 mmol) at –78 °C for 20 min. To the resultant mixture was added **3** (109 mg, 0.126 mmol) dissolved in THF (10 mL) and the mixture was stirred for 2 h at room tempera-

ture. Filtration through an alumina pad, evaporation of the volatiles and crystallization of the residue from toluene/ether gave **6a** as yellow crystals (71.6 mg, 0.0842 mmol, 67% yield). **6a** (64% yield): δ_H (CDCl₃) 7.9–7.4 (20H, m, Ph), 7.72, 7.05 (2H × 2, d × 2, J = 8.2 Hz, C₆H₄), 5.64 (1H, s, pyrazole ring proton), 2.82, 2.33 (4H × 2, br × 2, CH₂CH₂). δ_P (CDCl₃) 30.4 (d, J = 147 Hz). IR (KBr) 1980, 1958 cm⁻¹. FD-MS: m/z = 868 (M⁺). SiMe₃ derivative (**6b**): Complex **6b** was prepared in a manner similar to the synthesis of **6a**. **6b** (67% yield): δ_H (CDCl₃) 7.8–7.3 (20H, m, Ph), 5.58 (1H, s, pyrazole ring proton), 2.85, 2.27 (4H × 2, br × 2, CH₂CH₂), 0.30 (9H, s, SiMe₃). δ_P (CDCl₃) 29.6 (d, J = 145 Hz). IR (KBr) 1980, 1968, 1932 cm⁻¹. FD-MS: m/z = 850 (M⁺). *H* derivative (**6c**): Treatment of a THF solution (5 mL) of **6b** (54 mg, 0.063 mmol) with Bu₄N-F (a 1M THF solution, 63 μL, 0.0063 mmol) for 2 h at room temperature followed by evaporation of the volatiles, extraction with CH₂Cl₂ and filtration through an alumina pad gave **6c** (31 mg, 0.040 mmol, 63% yield) as yellow crystals after removal of the volatiles. **6c**: δ_H (CDCl₃) 7.9–7.3 (20H, m, Ph), 5.63 (1H, s, pyrazole ring proton), 3.38 (1H, s, ≡CH), 2.81, 2.26 (4H × 2, br × 2, CH₂CH₂). δ_P (CDCl₃) 30.4 (d, J = 144 Hz).

3.8. Preparation of [(μ-PNNP^{C2})₂{Rh(CO)}₄(μ-C≡C-R)]BF₄ (**7**)

p-Tol derivative (**7a**): An acetone solution (10 mL) of a mixture of **3** (29 mg, 0.040 mmol) and **6a** (33 mg, 0.039 mmol) was refluxed for 1 h. The obtained dark red solution was concentrated and addition of hexane caused precipitation of the product **7a** (50 mg, 0.029 mmol, 72% yield) as black solid. **7a**: δ_H (CDCl₃) 7.67, 7.06 (2H × 2, d × 2, J = 7.7 Hz, *p*-tol), 7.6–6.9 (40H, m, Ph), 5.52 (2H, s, pyrazole ring proton), 2.8–2.3 (16H, br, CH₂), 2.38 (3H, s, CH₃). δ_P (CDCl₃) 29.8 (d, J = 176 Hz). IR (KBr) 2003, 1977 cm⁻¹. ESI-MS: m/z = 1622 (M⁺ for the cationic part). SiMe₃ derivative (**7b**): Complex **7b** was prepared in a manner analogous to the synthesis of **7a**. **7b**: δ_H (CDCl₃) 7.9–7.4 (40H, m, Ph), 5.47 (2H, s, pyrazole ring proton), 3.0–2.4 (16H, br, CH₂), 0.21 (9H, s, SiMe₃). δ_P (CDCl₃) 28.9 (d, J = 176 Hz). *H* derivative (**7c**): Complex **7c** was prepared in a manner analogous to the synthesis of **7a**. **7c**: δ_H (CDCl₃) 7.5–7.3 (40H, m, Ph), 7.00 (1H, s, ≡CH), 5.47 (2H, s, pyrazole ring proton), 2.6–2.5 (16H, br, CH₂). δ_P (CDCl₃) 27.2 (d, J = 170 Hz). IR (KBr) 2007, 1982 cm⁻¹. ESI-MS: m/z = 1531 (M⁺ for the cationic part).

3.9. Preparation of [(μ-PNNP^{C2})₂{Rh(CO)}₄(μ₄-C₂)] (**8**)

To an acetone solution (5 mL) of **7c** (35 mg, 0.021 mmol) was added NEt₃ (3 mL). After the mixture was stirred for 1 h, the product **8** was precipitated by addition of hexane. **8** (22 mg, 0.014 mmol, 65% yield): δ_H (CDCl₃) 7.8–7.2 (40H, m, Ph), 5.68 (2H, s, pyrazole ring proton), 2.8–2.2 (16H, br, CH₂). δ_P (CDCl₃) 30.9 (d, J = 150 Hz). IR (KBr) 1982 cm⁻¹. ESI-MS: m/z = 1531 (M⁺ for the cationic part).

3.10. Preparation of [(μ-PNNP^{C2})₂{Rh(CO)}₄(μ₄-H)] (**9**)

To a THF solution (5 mL) of **3** (105 mg, 0.12 mmol) was added a THF solution (5 mL) of HSiEt₃ (19.4 mL, 0.120 mmol). After the mixture was stirred for 1.5 h, the product **9** was precipitated by addition of ether. **9** (73 mg, 0.046 mmol, 76% yield): δ_H (CDCl₃) 7.8–7.5 (40H, m, Ph), 5.70 (2H, s, pyrazole ring proton), 2.7 (16H, br, CH₂), –9.77 (1H, m, ¹J_{Rh-H} = 31.2 Hz, ¹J_{Rh-P} = 75.5 Hz, ²J_{H-P} = 13.6 Hz). δ_P (CDCl₃) 37.9 (d, J = 194 Hz). IR (KBr) 1980 cm⁻¹. ESI-MS: m/z = 1507 (M⁺ for the cationic part).

Acknowledgments

We are grateful to the Ministry of Education, Culture, Sports, Science and Technology of the Japanese Government and the Japan

Society for Promotion of Science and Technology for financial support of this research (Grants-in-Aid for Scientific Research: 20044007, and 22350026).

Appendix A. Supplementary material

CCDC 811872, 811873, 811874, and 8118725 contain the supplementary crystallographic data for (2), (3), (6a), and (6b). These data can be obtained free of charge from The Cambridge Crystallographic Data Centre via www.ccdc.cam.ac.uk/data_request/cif.

References

- [1] A.L. Gavrilova, B. Bosnich, *Chem. Rev.* 104 (2004) 349.
- [2] U. Beckmann, S. Brooker, *Coord. Chem. Rev.* 245 (2003) 1.
- [3] M.H. Klingele, S. Brooker, *Coord. Chem. Rev.* 241 (2003) 119.
- [4] J. Klingele, S. Dechert, F. Meyer, *Coord. Chem. Rev.* 253 (2009) 2698.
- [5] P. Braunstein, L.A. Oro, P.R. Raithby, *Metal Clusters in Chemistry*, vol. 3, Wiley-VCH, Weinheim, 1999.
- [6] P.J. Dyson, J.S. McIndoe, *Transition Metal Carbonyl Cluster Chemistry*, Gordon and Breach Science, Amsterdam, 2000.
- [7] D.F. Shriver, H.D. Kaesz, R.D. Adams, *The Chemistry of Metal Cluster Complexes*, VCH, New York, 1990.
- [8] E.W. Abel, F.G.A. Stone, G. Wilkinson, *Comprehensive Organometallic Chemistry II*, vols. 3–10, Pergamon, Oxford, 1995.
- [9] D.M.P. Mingos, R.H. Crabtree, *Comprehensive Organometallic Chemistry III*, vols. 4–8, Elsevier, Oxford, 2007.
- [10] (a) T.G. Schenk, J.M. Downs, C.R.C. Milne, P.B. Mackenzie, H. Boucher, J. Whelan, B. Bosnich, *Inorg. Chem.* 24 (1985) 2334;
(b) T.G. Schenk, C.R.C. Milne, J.F. Sawyer, B. Bosnich, *Inorg. Chem.* 24 (1985) 2338;
(c) B. Bosnich, *Inorg. Chem.* 38 (1999) 2554.
- [11] (a) S. Tanaka, M. Akita, *Angew. Chem., Int. Ed.* 40 (2001) 2865;
(b) S. Tanaka, C. Dubs, A. Inagaki, M. Akita, *Organometallics* 23 (2004) 317;
(c) C. Dubs, A. Inagaki, M. Akita, *Chem. Commun.* (2004) 2760;
(d) S. Tanaka, C. Dubs, A. Inagaki, M. Akita, *Organometallics* 24 (2005) 163;
(e) C. Dubs, T. Yamamoto, A. Inagaki, M. Akita, *Organometallics* 25 (2006) 1344;
(f) C. Dubs, T. Yamamoto, A. Inagaki, M. Akita, *Organometallics* 25 (2006) 1359;
(g) C. Dubs, T. Yamamoto, A. Inagaki, M. Akita, *Chem. Commun.* (2006) 1962.
- [12] T. Yamaguchi, T. Koike, M. Akita, *Organometallics* 29 (2010) 6493.
- [13] D.B. Grotjahn, S. Van, D. Combs, D.A. Lev, C. Schneider, M. Rideout, C. Meyer, G. Hernandez, L. Mejorado, *J. Org. Chem.* 67 (2002) 9200.
- [14] S. Reim, V.T.H. Nguyen, U. Albrecht, P. Langer, *Tetra. Lett.* 46 (2005) 8423.
- [15] M. Kimura, A. Ezo, M. Mori, K. Iwata, Y. Tamaru, *J. Am. Chem. Soc.* 128 (2006) 8559.
- [16] T.H. Chan, P. Brownbridge, *J. Am. Chem. Soc.* 102 (1980) 3534.
- [17] Y. Tanaka, T. Ishisaka, A. Inagaki, T. Koike, C. Lapinte, M. Akita, *Chem. Eur. J.* 16 (2010) 4762.